PHYSICAL REVIEW D **95,** 055023 (2017)

Probing the MSSM explanation of the muon g-2 anomaly in dark matter experiments and at a 100 TeV *pp* collider

Archil Kobakhidze,[1,†] Matthew Talia,[1,‡] and Lei Wu[1,2,*]

[1]*ARC Centre of Excellence for Particle Physics at the Terascale, School of Physics, The University of Sydney, New South Wales 2006, Australia*

[2]*Department of Physics and Institute of Theoretical Physics, Nanjing Normal University, Nanjing, Jiangsu 210023, China*

(Received 28 December 2016; published 27 March 2017)

We explore the ability of current and future dark matter and collider experiments in probing the anomalous magnetic moment of the muon, $(g-2)_\mu$, within the minimal supersymmetric standard model (MSSM). We find that the latest PandaX-II/LUX-2016 data give a strong constraint on parameter space that accommodates the $(g-2)_\mu$ within the 2σ range, which will be further excluded by the upcoming XENON-1T (2017) experiment. We also find that a 100 TeV pp collider can cover most of our surviving samples that satisfy dark matter (DM) relic density within the 3σ range through the Z or h resonant effect by searching for trilepton events from $\tilde{\chi}_2^0\tilde{\chi}_1^+$ associated production. The samples that are beyond future sensitivity of the trilepton search at a 100 TeV pp collider and the DM direct detections are either Higgsino/winolike lightest supersymmetric partilces (LSPs) or binolike LSPs coannihilating with sleptons. Such compressed regions may be covered by the monojet(like) searches at a 100 TeV pp collider.

DOI: 10.1103/PhysRevD.95.055023

I. INTRODUCTION

The discovery of the Higgs boson [1,2] and subsequent measurements of its properties completed the Standard Model (SM) and provided it with very convincing evidence for the simplest perturbative realization of the electroweak symmetry breaking (EWSB). Despite this overwhelming empirical success, our understanding of EWSB is incomplete. Namely, the quantum corrections are known to drive the Higgs mass (and hence the electroweak scale) toward high-energy scales, and thus the SM requires unnaturally precise fine-tuning of parameters to satisfy the observations. In addition, observations of neutrino oscillations and dark matter (DM) certainly require beyond the standard model physics.

Other deviations from the SM prediction are long seen in the measurements of the anomalous magnetic moment of the muon, $a_\mu = (g-2)_\mu/2$ [3–6]. The recently measured values [7–9],

$$\Delta a_\mu^{\text{Exp-SM}} = \begin{cases} (28.7 \pm 8.0) \times 10^{-10}, \\ (26.1 \pm 8.0) \times 10^{-10}, \end{cases} \tag{1}$$

are more than 3σ away from the SM prediction, which includes improved QED [10] and electroweak [11] contributions. The upcoming experiments at NBL will measure the $(g-2)_\mu$ with a precision of 0.14 ppm [12], which would potentially allow a 5σ discovery of new physics through such measurements. Needless to say, there are several candidate explanations for the $(g-2)_\mu$ anomaly proposed within various new physics frameworks.

The weak-scale supersymmetry (SUSY) has long been the dominant paradigm for new particle physics. The minimal supersymmetric standard model (MSSM) not only provides an elegant solution to the hierarchy problem but also may successfully explain the $(g-2)_\mu$ anomaly [13–33]. In the MSSM, the most significant contribution to a_μ is due to the one-loop diagrams involving the smuon $\tilde{\mu}$, muon sneutrino $\tilde{\nu}_\mu$, neutralinos $\tilde{\chi}^0$, and charginos $\tilde{\chi}^\pm$. The one-loop contribution to a_μ arises if there is a chirality flip between incoming and outgoing external muon lines, which may be induced through the $L-R$ mixing in the smuon sector or the SUSY Yukawa couplings of Higgsinos to the muon and $\tilde{\mu}$ or $\tilde{\nu}_\mu$. Therefore, these contributions to a_μ are typically proportional to $m_\mu^2/M_{\text{SUSY}}^2$. Thus, to generate the sizable contributions to a_μ, the SUSY scale M_{SUSY} encapsulating slepton and electroweakino masses has to be around $O(100)$ GeV. So, the detection of light sleptons and electroweakinos will provide a test for the MSSM solution to the $(g-2)_\mu$ problem.

The negative results of direct searches for sparticles during the LHC Run-1 have pushed up the mass limits of the first two generation squarks and gluino into the TeV region [34,35]. The third generation squarks have been tightly constrained in the simplified models [36,37], such as in stealth SUSY [38] and natural SUSY [39–44]. Unlike the colored sparticles, the bounds on the sleptons [45,46] and electroweakinos [47,48] are relatively weak, especially for the region of the compressed spectrum. The lightest

*Corresponding author.
lei.wu1@sydney.edu.au
†archil.kobakhidze@sydney.edu.au
‡matthew.talia@sydney.edu.au

neutralino still remains as a successful DM candidate, and a significant effort has been made to obtain a lower mass limit on the neutralino LSP in MSSM; see, e.g., [49–52].

In this paper, we explore the potential of the current and future dark matter and collider experiments to probe the anomalous magnetic moment of the muon within the MSSM. Using LEP and Higgs data and demanding that the theory accommodates $(g-2)_\mu$ measurements within the 2σ range, we derive bounds on the electroweakino masses. Following this, we impose dark matter constraints from Planck, PandaX-II/LUX 2016 data, and constraints from LHC searches for dilepton and trilepton events. Then, we evaluate the prospect of a future 100 TeV hadron collider in probing electroweakinos in trilepton events within this scenario. Finally, our conclusions are presented.

II. $(g-2)_\mu$ IN MSSM

The low-energy effective operator for magnetic dipole moment (MDM) is given by

$$\mathcal{L}_{\rm MDM} = \frac{e}{4m_\mu} a_\mu \bar{\mu}\sigma_{\rho\lambda}\mu F^{\rho\lambda}, \tag{2}$$

where e is the electric charge and m_μ is the muon mass. $F^{\rho\lambda}$ is the field strength of the photon field and $\sigma_{\rho\lambda} = \frac{i}{2}[\gamma_\rho, \gamma_\lambda]$.

In the MSSM, there are essentially two types of diagrams that contribute to a_μ at one-loop; i.e., one is the $\tilde{\chi}^0 - \tilde{\mu}$ loop diagram (left panel of Fig. 1) and the other is the chargino $\tilde{\chi}^\pm - \tilde{\nu}_\mu$ loop diagram (right panel of Fig. 1). The expressions for one-loop SUSY corrections to a_μ (including the complex phases effects) are given by [14]

$$a_\mu^{\tilde{\chi}^0} = \frac{m_\mu}{16\pi^2}\sum_{i,\alpha}\left\{-\frac{m_\mu}{12m^2_{\tilde{\mu}_m}}(|n^L_{i\alpha}|^2 + |n^R_{i\alpha}|^2)F_1^N(x_{i\alpha}) + \frac{m_{\tilde{\chi}^0_i}}{3m^2_{\tilde{\mu}_m}}\mathrm{Re}(n^L_{i\alpha}n^R_{i\alpha})F_2^N(x_{i\alpha})\right\}, \tag{3}$$

$$a_\mu^{\tilde{\chi}^+} = \frac{m_\mu}{16\pi^2}\sum_{j}\left\{\frac{m_\mu}{12m^2_{\tilde{\nu}_\mu}}(|c^L_j|^2 + |c^R_j|^2)F_1^C(x_j) + \frac{2m_{\tilde{\chi}^\pm_j}}{3m^2_{\tilde{\nu}_\mu}}\mathrm{Re}(c^L_j c^R_j)F_2^C(x_j)\right\}, \tag{4}$$

where $i = 1, 2, 3, 4$; $j = 1, 2$; and $\alpha = 1, 2$ denotes the neutralino, chargino, and smuon mass eigenstates, respectively. The couplings are defined as

$$\begin{aligned} n^R_{i\alpha} &= \sqrt{2}g_1 N_{i1}X_{\alpha 2} + y_\mu N_{i3}X_{\alpha 1},\\ n^L_{i\alpha} &= \frac{1}{\sqrt{2}}(g_2 N_{i2} + g_1 N_{i1})X^*_{\alpha 1} - y_\mu N_{i3}X^*_{\alpha 2},\\ c^R_j &= y_\mu U_{j2},\\ c^L_j &= -g_2 V_{j1}, \end{aligned} \tag{5}$$

where the muon Yukawa coupling $y_\mu = g_2 m_\mu/\sqrt{2}m_W \cos\beta$. N are the neutralino and U, V are the chargino mixing matrices, respectively. X denotes the slepton mixing matrix. In terms of the kinematic variables $x_{i\alpha} = m^2_{\tilde{\chi}^0_i}/m^2_{\tilde{\mu}_\alpha}$ and $x_j = m^2_{\tilde{\chi}^\pm_j}/m^2_{\tilde{\nu}_\mu}$, the loop functions F are defined as follows:

$$\begin{aligned} F_1^N(x) &= \frac{2}{(1-x)^4}[1 - 6x + 3x^2 + 2x^3 - 6x^2\ln x],\\ F_2^N(x) &= \frac{3}{(1-x)^3}[1 - x^2 + 2x\ln x],\\ F_1^C(x) &= \frac{2}{(1-x)^4}[2 + 3x - 6x^2 + x^3 + 6x\ln x],\\ F_2^C(x) &= -\frac{3}{2(1-x)^3}[3 - 4x + x^2 + 2\ln x]. \end{aligned} \tag{6}$$

These one-loop corrections mainly rely on the bino/wino masses $M_{1,2}$, the Higgsino mass μ, the left- and right-smuon mass parameters, $M_{\tilde{\mu}_L,\tilde{\mu}_R}$, and the ratio of the two Higgs vacuum expectation values, $\tan\beta$. They have a weak dependence on the second generation trilinear coupling A_μ. In the limit of large $\tan\beta$, when all the mass scales are roughly of the same order of $M_{\rm SUSY}$, the contributions Eq. (3) and Eq. (4) can be approximately written as

$$a_\mu^{\tilde{\chi}^\pm} \simeq \frac{m_\mu^2 g_2^2}{32\pi^2 M^2_{\rm SUSY}}\tan\beta; \tag{7}$$

$$a_\mu^{\tilde{\chi}^0} \simeq \frac{m_\mu^2}{192\pi^2 M^2_{\rm SUSY}}(g_1^2 - g_2^2)\tan\beta. \tag{8}$$

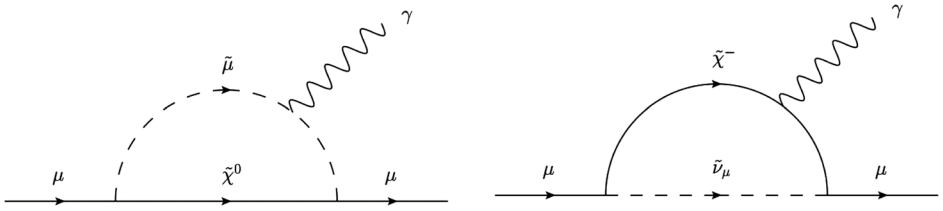

FIG. 1. One-loop diagram contributions of the MSSM to the muon anomalous magnetic moment, $(g-2)_\mu$. The first involves a smuon-neutralino (left) and the second a chargino-muon sneutrino loop (right).

The detailed dependence of a_μ on the five relevant mass parameters $\tan\beta$ is complicated. For two-loop corrections, it should be noted that if the squark masses (or masses of the first or third generation slepton) become large, the SUSY contributions to a_μ do not decouple but are logarithmically enhanced. Depending on the mass pattern, a positive or negative correction of O(10%) for squark masses in the few TeV region can be obtained; see Ref. [53].

III. CONSTRAINTS ON MSSM EXPLANATION OF $(g-2)_\mu$

In the following, we numerically calculate Δa_μ by using the FeynHiggs-2.12.0 [54] package and scan the relevant MSSM parameter space:

$$10 < \tan\beta < 50, \quad -2\ \text{TeV} < M_1, \quad M_2 < 2\ \text{TeV},$$
$$-2\ \text{TeV} < \mu < 2\ \text{TeV}, \quad 0.1\ \text{TeV} < m_{\tilde{l}_L}, \quad m_{\tilde{l}_R} < 2\ \text{TeV}, \tag{9}$$

where we have the subscript $\ell = e, \mu$. Because of the small effects on a_μ, the slepton trilinear parameters of the first two generations are assumed as $A_\ell = 0$. We also decouple the stau sector by setting the soft stau mass parameters $m_{\tilde{\tau}_L} = m_{\tilde{\tau}_R} = 5$ TeV and trilinear parameter $A_\tau = 0$. So the stau will not contribute to the trilepton signals in our simulations. To satisfy the 125 GeV Higgs mass within a 2 GeV deviation, we vary the stop trilinear parameter in the range $|A_t| < 5$ TeV and set the stop soft masses at 5 TeV. We require the mixing parameter $|X_t/M_S| < 2$ to avoid the charge/color-breaking minima [55]. We additionally calculate the Higgs mass and the rest of the sparticle masses with FeynHiggs-2.12.0 [54].

A. LEP and Higgs data

In our scan, we also consider the following experimental bounds:

(i) LEP: the direct searches for the slepton and chargino at LEP produce the lower mass limits on the first two generation sleptons and lightest chargino [56],

$$m_{\tilde{l}_L}, m_{\tilde{l}_R} > 100\ \text{GeV} \qquad (l = e, \mu), \tag{10}$$

$$m_{\tilde{\chi}_1^\pm} > 105\ \text{GeV}. \tag{11}$$

(ii) Higgs data: the exclusion limits at 95% C.L. from the experimental cross sections from Higgs searches at LEP, Tevatron, and LHC are examined by using HiggsBounds-4.2.1 [57].

(iii) We require the lightest neutralino $\tilde{\chi}_1^0$ as the LSP and $m_{\tilde{\chi}_1^0} > 30$ GeV to be consistent with the bound on light MSSM neutralino dark matter [58].

In Fig. 2, we present the dependence of Δa_μ on the masses of neutralinos ($\tilde{\chi}_{1,2}^0$), charginos ($\tilde{\chi}_{1,2}^\pm$), and smuons ($\tilde{\mu}_{1,2}$). Within the scan ranges of Eq. (9), we find that the $\tilde{\chi}^\pm - \tilde{\nu}_\mu$ loop dominates over the $\tilde{\chi}^0 - \tilde{\mu}$ loop. A sizable SUSY contribution to a_μ can be obtained, if M_1, M_2, and μ have the same sign and $\tilde{\chi}_{1,2}^0$ and $\tilde{\chi}_1^\pm$ have sizable Higgsino, wino, or both components with large $\tan\beta$. The explanation of Δa_μ within a 2σ range requires $m_{\tilde{\chi}_1^0} < 1.0$ TeV and $m_{\tilde{\mu}_1} < 1.03$ TeV.[1] However, a Higgsino or winolike LSP typically cannot satisfy the constraints of the dark matter relic density and are constrained using data from direct detection experiments.

B. DM relic density and direct detection experiments

Next, we confront the MSSM explanation of $(g-2)_\mu$ with the various dark matter experiments. We use MicrOmegas-4.2.3 [62] to calculate the dark matter relic density Ωh^2 and the spin-independent neutralino scattering cross sections with nuclei, denoted as σ^{SI}. It should be noted that the thermal relic abundance of the light Higgsino or winolike neutralino dark matter is typically low due to the large annihilation rate in the early universe. This leads to the standard thermally produced Weakly Interacting Massive Particle(WIMP) dark matter being underabundant. In order to have the correct relic density, several alternatives have been proposed, such as choosing the axion-Higgsino admixture as a dark matter candidate [63]. So we rescale the scattering cross section σ^{SI} by a factor of $(\Omega h^2/\Omega_{\text{Planck}} h^2)$, where $\Omega_{\text{Planck}} h^2 = 0.112 \pm 0.006$ is the relic density measured by the Planck satellite [64].

In Fig. 3, we show the neutralino dark matter relic density Ωh^2 (left) and the spin-independent neutralino-nucleon scattering cross section σ^{SI} (right). All samples satisfy the LEP, Higgs data, and $(g-2)_\mu$ within 2σ. In the left panel of Fig. 3, it can be seen that there are a number of samples above the 3σ upper bound of the Planck relic density measurement. Those samples are binolike and annihilate to the SM particles very slowly, which leads to an overabundance of dark matter in the universe. On the other hand, there are two dips around M_Z and M_h, respectively, where $\tilde{\chi}_1^0\tilde{\chi}_1^0$ can efficiently annihilate through the resonance effect. When the LSP Higgsino or wino component dominates, the annihilation cross section of $\tilde{\chi}_1^0\tilde{\chi}_1^0$ is small so that the relic density is less than the 3σ lower bound of the Planck value. A mixed LSP with a certain Higgsino or wino fraction [61] can be reconciled

[1] It should be noted that if the Higgsino mass parameter μ is large enough, the $g-2$ anomaly may be explained through the bino-smuon loop contribution, due to the large smuon left-right mixing [59]. But such a large μ scenario is disfavored by the vacuum stability [59] and the naturalness [60] and is highly constrained by the dark matter relic density [61].

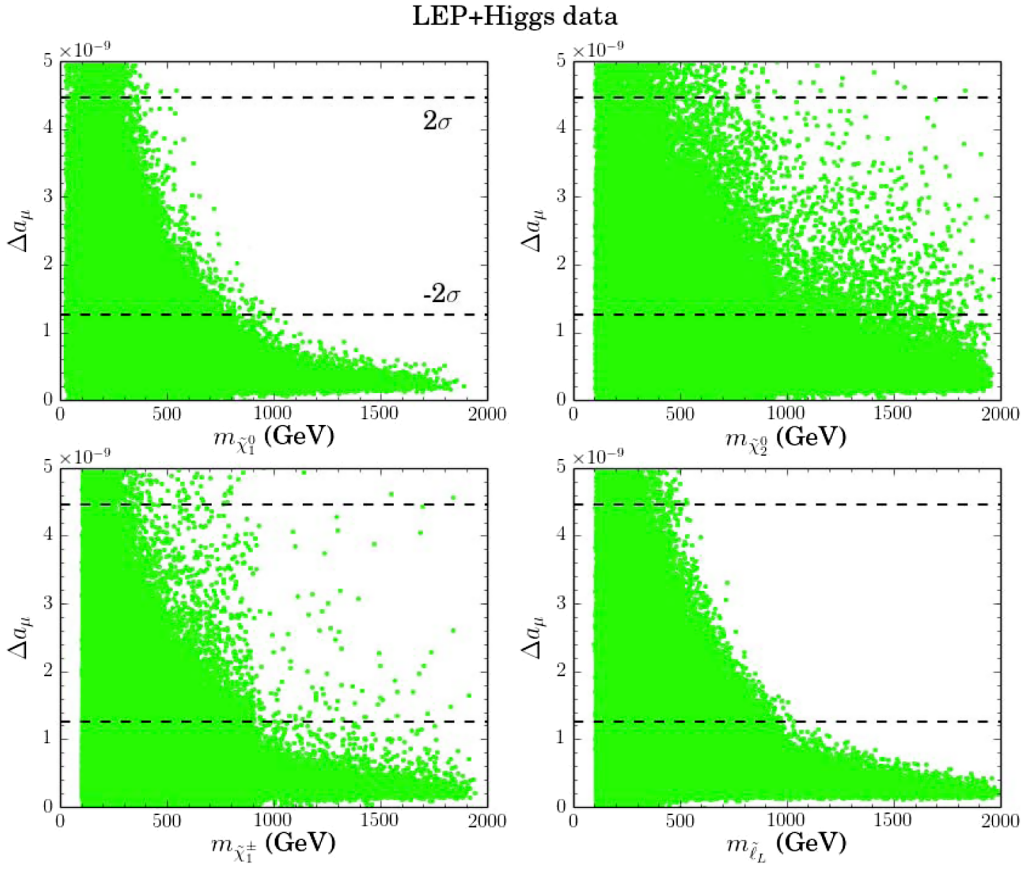

FIG. 2. Scatter plot on the plane of Δa_μ and sparticle masses. Green circles satisfy the constraints from LEP and LHC Higgs data. The dashed lines represent the 2σ band on Δa_μ given by Eq. (1).

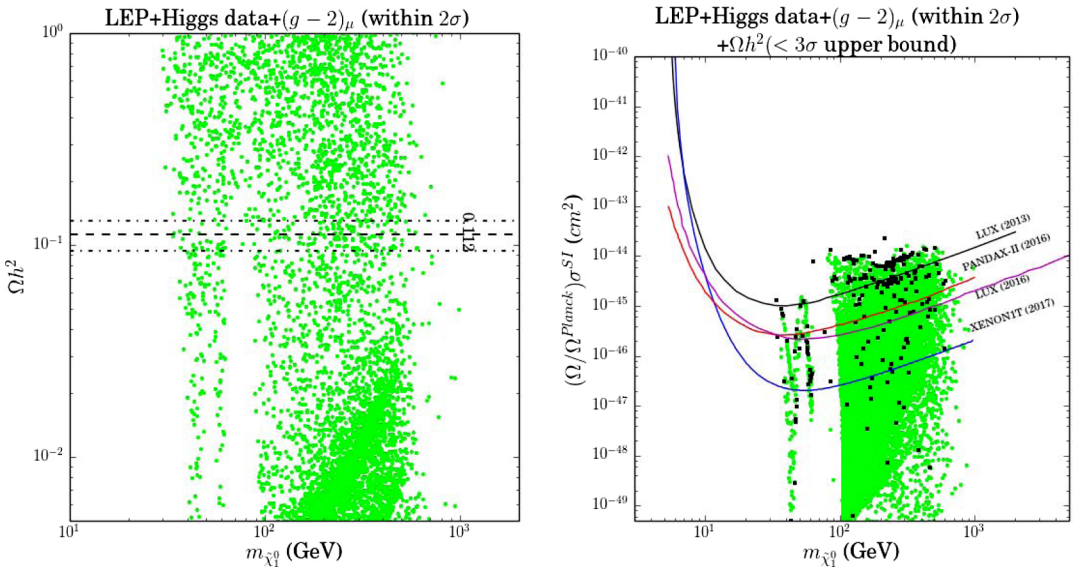

FIG. 3. The neutralino dark matter relic density Ωh^2 (left) and the spin-independent neutralino-nucleon scattering cross section $\sigma^{\rm SI}$ (right). The dashed line is the PLANCK central value, and the dash-dotted lines are corresponding 3σ bands. The exclusion limits on the $\sigma^{\rm SI}$ from LUX (2013) (black line) [65], LUX (2016) (magenta line) [66], PandaX-II (red line) [67], and XENON1T (2017) (blue line) [68] are projected. Green circles satisfy the LEP, Higgs data, and 2σ bound of $(g-2)_\mu$ (left) and 3σ upper bound of Ωh^2, while the black squares further require Ωh^2 within the 3σ range.

with the measured relic abundance Ωh^2 within the 3σ range. In the right panel of Fig. 3, we project the samples that satisfy 3σ upper bound $\Omega_{\rm Planck}h^2$ on the plane of $\sigma^{\rm SI}$ versus $m_{\tilde{\chi}_1^0}$.

A significant portion of the parameter space where the LSP has a sizable Higgsino or wino component is excluded by the recent PandaX-II [67] and LUX data [66]. The samples with nearly pure Higgsino or wino LSPs escape experimental constraints due to the large reduction in the DM abundance. We also find some samples with the correct DM relic density (within 3σ) that satisfy the LUX constraints. These samples can be placed in two categories. The smaller portion of samples belong to the so-called MSSM blind-spot region of parameters [69,70] where the LSP coupling to the Higgs/Z boson is so small that the DM-nucleon scattering cross section is highly suppressed. The sfermions and other heavy Higgs bosons are decoupled for these particular samples. The second case is that the binolike LSPs coannihilate with the sleptons. The scattering cross section of the binolike LSP with the nucleon can be small to avoid the LUX bound. The future XENON1T (2017) experiment [68] will further cover the parameter space.

C. LHC 8 TeV collider search

Given the great progress of LHC experiments, we recast the results of searching for $2\ell + \not{E}_T$ and $3\ell + \not{E}_T$ signatures at LHC-8 TeV. We focus on 8 TeV data. In fact, most of the dedicated analyses at 13 TeV are either preliminary [71–73] or do not provide stronger constraints in general due to the still small luminosity [74]. The main processes contributing to $2\ell + \not{E}_T$ events can arise from the production of sleptons pair and charginos,

$$pp \to \tilde{\ell}^+\tilde{\ell}^-, \tilde{\chi}_1^+\tilde{\chi}_1^- \tag{12}$$

with the subsequent decays to leptons:

(i) slepton decay: $\tilde{\ell}^\pm \to \ell^\pm\tilde{\chi}_1^0$;

(ii) chargino decays: (a) through sleptons: $\tilde{\chi}_1^\pm \to \tilde{\ell}^\pm(\to \ell^\pm\tilde{\chi}_1^0)\nu_\ell$, (b) through sneutrinos: $\tilde{\chi}_1^\pm \to \tilde{\nu}_\ell(\to \nu_\ell\tilde{\chi}_1^0)\ell^\pm$, (c) through W boson: $\tilde{\chi}_1^\pm \to W^\pm(\to \ell^\pm\nu_\ell)\tilde{\chi}_1^0$.

While $3\ell + \not{E}_T$ events mainly come from the associated production of chargino and neutralino,

$$pp \to \tilde{\chi}_i^0\tilde{\chi}_j^\pm, \tag{13}$$

where $i = 2, 3, 4$ and $j = 1, 2$. They then decay in two different ways:

(i) through sleptons/sneutrinos: (a) $\tilde{\chi}_i^0 \to \ell^\mp\tilde{\ell}^\pm(\to \ell^\pm\tilde{\chi}_1^0)$, $\tilde{\chi}_j^\pm \to \tilde{\ell}^\pm(\to \ell^\pm\tilde{\chi}_1^0)\nu_\ell$, (b) $\tilde{\chi}_i^0 \to \ell^\mp\tilde{\ell}^\pm(\to \ell^\pm\tilde{\chi}_1^0)$, $\tilde{\chi}_j^\pm \to \tilde{\nu}_\ell(\to \nu_\ell\tilde{\chi}_1^0)\ell^\pm$;

(ii) through the SM gauge bosons: $\tilde{\chi}_i^0 \to Z^{(*)}(\to \ell^\pm\ell^\mp)\tilde{\chi}_1^0$, $\tilde{\chi}_j^\pm \to W^{\pm(*)}(\to \ell^\pm\nu_\ell)\tilde{\chi}_1^0$.

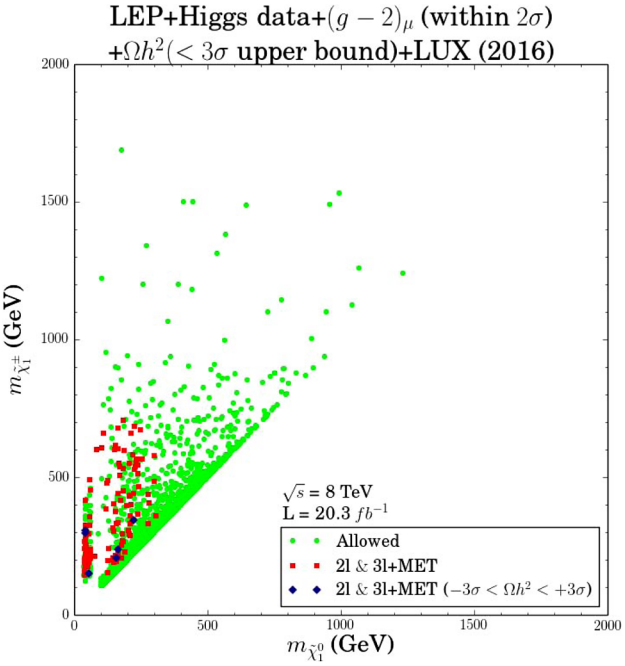

FIG. 4. Exclusion limits from LHC Run-1 dilepton and trilepton events. All samples satisfy the LEP, Higgs data, 3σ upper bound of the dark matter relic density, LUX 2016, and $(g-2)_\mu$ within the 2σ. Red squares ($\Omega h^2 < +3\sigma$) and blue diamonds ($-3\sigma < \Omega h^2 < +3\sigma$) are excluded by $2\ell + \not{E}_T$ and $3\ell + \not{E}_T$ events.

We use SPheno-3.3.8 [75] to produce the spectrum file to employ in MadGraph5_aMC@NLO [76] and generate the parton level signal events. Then the events are showered and hadronized by PYTHIA [77]. The detector effects are included by using the tuned Delphes [78]. FastJet [79] is used to cluster jets with the anti-k_t algorithm [80]. We recast the ATLAS dilepton [45] and trilepton [47] analyses by using CheckMATE-1.2.2 [81]. We include the next-to-leading order correction effects in the production of $\tilde{\ell}^\pm\tilde{\ell}^\mp$, $\tilde{\chi}_i^\pm\tilde{\chi}_i^\mp$, and $\tilde{\chi}_i^0\tilde{\chi}_j^\pm$ productions by multiplying a K-factor 1.3 [82]. The main SM backgrounds include WZ, ZZ, and $ttV(V = W, Z)$. To estimate the exclusion limit, we define the ratio $r = \max(N_{S,i}/S^{95\%}_{{\rm obs},i})$, where $N_{S,i}$ and $S^{95\%}_{{\rm obs},i}$ are the event numbers of the signal for the ith signal region and the corresponding observed 95% C.L. upper limit, respectively. The max is over all signal regions defined in the analysis. We conclude that a sample is excluded at 95% C.L., if $r > 1$.

In Fig. 4, we recast the LHC Run-1 dilepton and trilepton exclusion limits on the plane of $m_{\tilde{\chi}_1^\pm}$ and $m_{\tilde{\chi}_1^0}$. All samples satisfy the LEP, Higgs data, 3σ upper bound of relic density, LUX 2016, and $(g-2)_\mu$ within the 2σ range. Red squares ($\Omega h^2 < +3\sigma$) and blue diamonds ($-3\sigma < \Omega h^2 < +3\sigma$) are excluded by $2\ell + \not{E}_T$ and $3\ell + \not{E}_T$ events. In Fig. 4, we can see that a portion of samples in $\tilde{\chi}_1^\pm < 710$ GeV and $\tilde{\chi}_1^0 < 300$ GeV can be excluded. A bulk of samples in the parameter space with $\tilde{\chi}_1^0$ being Higgsino or winolike cannot

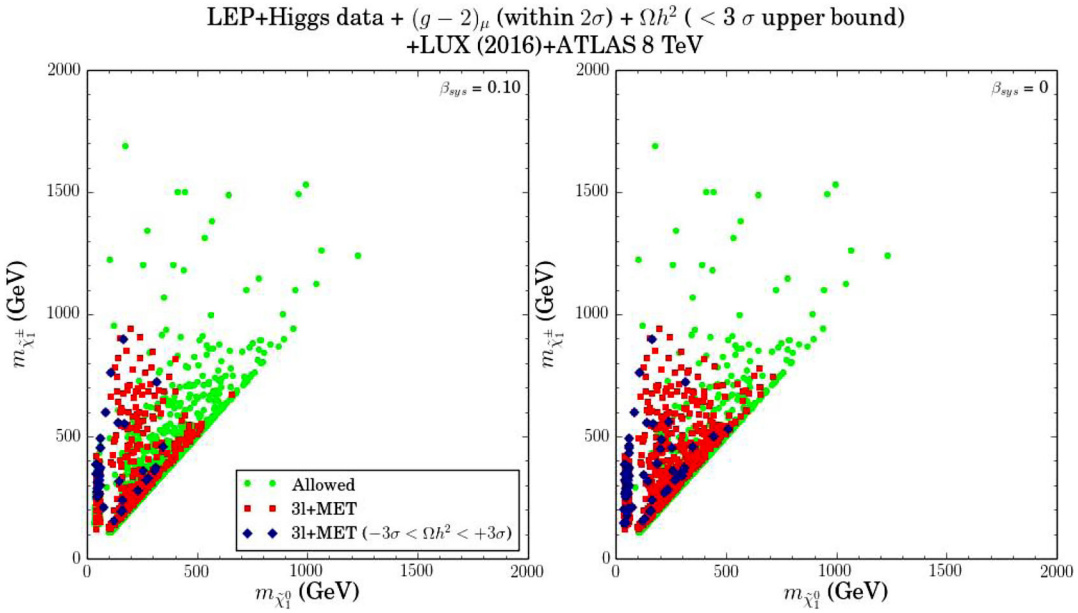

FIG. 5. Same as Fig. 4, but for the expected exclusion limit at a 100 TeV pp collider with the luminosity of 3000 fb^{-1}. Red squares ($\Omega h^2 < +3\sigma$) and blue diamonds $-3\sigma < \Omega h^2 < +3\sigma$ are excluded by searching for $3\ell + \text{MET}$ events. The systematic uncertainty β_{sys} is taken as 0.1 and 0, respectively.

be covered because of the small mass difference between $\tilde{\chi}_1^\pm$ and $\tilde{\chi}_1^0$. Such a region may be accessed by the monojet (like) or the vector boson fusion production at HL-LHC [83–89]. In addition, when $\tilde{\chi}_2^0$ has a sizable bino component, the limit from trilepton events will become weak because of the reduction of the cross section of $\tilde{\chi}_1^\pm\tilde{\chi}_2^0$. We also find that the dilepton channel can be complementary to the trilepton channel when the latter is suppressed by small neutralino leptonic branching ratios. An important factor in the dilepton and trilepton yields is the leptonic branching fraction that can vary widely throughout the parameter space. If the slepton is on shell, the chargino two-body decays then dominate and its leptonic branching fraction is maximized, $\text{Br}(\tilde{\chi}_1^\pm \to \tilde{\chi}_1^0\tilde{\ell}^\pm(\to \ell^\pm\nu_\ell))_{\text{max}} = 2/3$. When the sneutrino is on shell and is lighter than the corresponding slepton, the channel $\tilde{\chi}_2^0 \to \nu_\ell\tilde{\nu}_\ell$ will dominate the decay width, and the neutralino leptonic branching ratio is suppressed. On the other hand, if the slepton and sneutrino are heavy enough, the decay amplitudes of $\tilde{\chi}_1^\pm$ and $\tilde{\chi}_2^0$ are dominated by W and Z boson exchanges, respectively, which give $\tilde{\chi}_1^\pm \to \tilde{\chi}_1^0 W^\pm(\to \ell^\pm\nu_\ell) \simeq 2/9$ and $\tilde{\chi}_2^0 \to \tilde{\chi}_1^0 Z$ $(\to \ell^\pm\ell^\mp) \simeq 6\%$. On the other hand, $\tilde{\chi}_2^0$ can decay to $h\tilde{\chi}_1^0$ with a sizable branching ratio if kinematically accessible, which can also weaken the trilepton exclusion limit.

IV. PROSPECTS AT A 100 TEV COLLIDER

To hunt for new fundamental particles, a 100 TeV pp collider has been under discussion in recent years, which will allow us to probe the new physics scale roughly an order of magnitude higher than we can possibly reach with the LHC [90]. In this section, we estimate the prospects of probing the MSSM explanation of the $(g-2)_\mu$ anomaly by extrapolating the above 8 TeV trilepton analysis to a 100 TeV pp collider. For each allowed sample above, we use the most sensitive signal region in 8 TeV analysis and simply assume the same detection efficiency in the 100 TeV analysis. We rescale the signal (S) and background (B) events by the following ratio:

$$N^{100\text{ TeV}} = (\sigma^{100\text{ TeV}}/\sigma^{8\text{ TeV}})(3000\text{ fb}^{-1}/20.3\text{ fb}^{-1})N^{8\text{ TeV}}. \tag{14}$$

Such a treatment can be considered as a preliminary theoretical estimation. The optimized analysis strategy may be achieved once the details of the collider environment is known. To obtain the expected exclusion limits, we use the following equation:

$$\frac{S}{\sqrt{B + (\beta_{\text{sys}}B)^2}} \geq 2 \quad [\text{excluded}], \tag{15}$$

where the factor β_{sys} parametrizes the systematic uncertainty. In Fig. 5, we can see that when $\beta_{\text{sys}} = 0.1$, a majority of samples allowed by $(g-2)_\mu$ in the parameter space with $\tilde{\chi}_1^0 < 530$ GeV and $\tilde{\chi}_1^\pm < 940$ GeV can be excluded. Such a range will be extended to $\tilde{\chi}_1^0 < 710$ GeV and $\tilde{\chi}_1^\pm < 940$ GeV, if $\beta_{\text{sys}} = 0$.

It should be noted that the region that satisfies the DM relic density within the 3σ range through the Z or h resonant annihilation in the blind spots can be covered by

searching for trilepton events from $\tilde{\chi}_2^0\tilde{\chi}_1^+$ associated production at a 100 TeV pp collider. The samples that are beyond future sensitivity of this trilepton search and the DM direct detections are either Higgsino/winolike LSPs with the compressed mass spectrum or binolike LSPs coannihilating with sleptons. Such compressed regions may be probed by the monojet(like) searches at a 100 TeV pp collider [91].

V. CONCLUSION

In this work we have studied the prospect of current and future dark matter and collider experiments in probing the anomalous magnetic moment of the muon in the MSSM. Under the constraints of Higgs data, dark matter relic density, PandaX-II/LUX-2016 experiments, and LHC-8 TeV searches for dilepton/trilepton events, we find the Planck data and the recent PandaX-II/LUX data can significantly exclude the MSSM parameter space satisfying $(g-2)_\mu$, which will be further excluded by the upcoming XENON-1T (2017) experiment. We also find that most of our surviving samples that satisfy DM relic density within the 3σ range through the Z or h resonant effect can be covered by searching for trilepton events from $\tilde{\chi}_2^0\tilde{\chi}_1^+$ associated production of a 100 TeV pp collider. While the samples that are beyond the future sensitivity of this trilepton search and DM direct detections are either Higgsino/winolike LSPs or binolike LSPs coannihilating with sleptons. Such compressed regions may be probed by the monojet(like) searches at a future 100 TeV pp collider.

ACKNOWLEDGMENTS

This work was partially supported by the Australian Research Council. L. W. was also supported in part by the National Natural Science Foundation of China (NNSFC) under Grants No. 11305049 and No. 11275057.

[1] G. Aad *et al.* (ATLAS Collaboration), Phys. Lett. B **716**, 1 (2012).
[2] S. Chatrchyan *et al.* (CMS Collaboration), Phys. Lett. B **716**, 30 (2012).
[3] K. Hagiwara, A. D. Martin, D. Nomura, and T. Teubner, Phys. Lett. B **557**, 69 (2003).
[4] F. Jegerlehner and A. Nyffeler, Phys. Rep. **477**, 1 (2009).
[5] J. P. Miller, E. de Rafael, B. L. Roberts, and D. Stöckinger, Annu. Rev. Nucl. Part. Sci. **62**, 237 (2012).
[6] T. Blum, A. Denig, I. Logashenko, E. de Rafael, B. L. Roberts, T. Teubner, and G. Venanzoni, arXiv:1311.2198.
[7] G. W. Bennett *et al.* (Muon $g-2$ Collaboration), Phys. Rev. D **73**, 072003 (2006).
[8] M. Davier, A. Hoecker, B. Malaescu, and Z. Zhang, Eur. Phys. J. C **71**, 1515 (2011); **72**, 1874(E) (2012).
[9] K. Hagiwara, R. Liao, A. D. Martin, D. Nomura, and T. Teubner, J. Phys. G **38**, 085003 (2011).
[10] T. Aoyama, M. Hayakawa, T. Kinoshita, and M. Nio, Phys. Rev. Lett. **109**, 111808 (2012).
[11] C. Gnendiger, D. Stöckinger, and H. Stöckinger-Kim, Phys. Rev. D **88**, 053005 (2013).
[12] G. Venanzoni (Fermilab E989 Collaboration), Nucl. Part. Phys. Proc. **273–275**, 584 (2016).
[13] T. Moroi, Phys. Rev. D **53**, 6565 (1996); **56**, 4424(E) (1997).
[14] S. P. Martin and J. D. Wells, Phys. Rev. D **64**, 035003 (2001).
[15] D. Stöckinger, J. Phys. G **34**, R45 (2007).
[16] G.-C. Cho, K. Hagiwara, Y. Matsumoto, and D. Nomura, J. High Energy Phys. 11 (2011) 068.
[17] M. Endo, K. Hamaguchi, S. Iwamoto, and T. Yoshinaga, J. High Energy Phys. 01 (2014) 123.
[18] M. Ibe, T. T. Yanagida, and N. Yokozaki, J. High Energy Phys. 08 (2013) 067.
[19] S. Akula and P. Nath, Phys. Rev. D **87**, 115022 (2013).
[20] S. Mohanty, S. Rao, and D. P. Roy, J. High Energy Phys. 09 (2013) 027.
[21] K. Kowalska, L. Roszkowski, E. M. Sessolo, and A. J. Williams, J. High Energy Phys. 06 (2015) 020.
[22] F. Wang, W. Wang, J. M. Yang, and Y. Zhang, J. High Energy Phys. 07 (2015) 138.
[23] F. Wang, W. Wang, and J. M. Yang, J. High Energy Phys. 06 (2015) 079.
[24] F. Wang, L. Wu, J. M. Yang, and M. Zhang, Phys. Lett. B **759**, 191 (2016).
[25] N. Okada, S. Raza, and Q. Shafi, Phys. Rev. D **90**, 015020 (2014).
[26] I. Gogoladze, F. Nasir, Q. Shafi, and C. S. Un, Phys. Rev. D **90**, 035008 (2014).
[27] K. S. Babu, I. Gogoladze, Q. Shafi, and C. S. Ün, Phys. Rev. D **90**, 116002 (2014).
[28] M. A. Ajaib, I. Gogoladze, Q. Shafi, and C. S. Ün, J. High Energy Phys. 05 (2014) 079.
[29] M. A. Ajaib, B. Dutta, T. Ghosh, I. Gogoladze, and Q. Shafi, Phys. Rev. D **92**, 075033 (2015).
[30] M. Adeel Ajaib, I. Gogoladze, and Q. Shafi, Phys. Rev. D **91**, 095005 (2015).
[31] I. Gogoladze, Q. Shafi, and C. S. Ün, Phys. Rev. D **92**, 115014 (2015).
[32] M. Badziak, Z. Lalak, M. Lewicki, M. Olechowski, and S. Pokorski, J. High Energy Phys. 03 (2015) 003.
[33] P. Athron, M. Bach, H. G. Fargnoli, C. Gnendiger, R. Greifenhagen, J.-h. Park, S. Paßehr, D. Stöckinger, H. Stöckinger-Kim, and A. Voigt, Eur. Phys. J. C **76**, 62 (2016).

[34] G. Aad *et al.* (ATLAS Collaboration), J. High Energy Phys. 10 (2013) 130; 01 (2014) 109(E).
[35] S. Chatrchyan *et al.* (CMS Collaboration), J. High Energy Phys. 06 (2014) 055.
[36] G. Aad *et al.* (ATLAS Collaboration), J. High Energy Phys. 11 (2014) 118.
[37] S. Chatrchyan *et al.* (CMS Collaboration), Eur. Phys. J. C **73**, 2677 (2013).
[38] J. Fan, R. Krall, D. Pinner, M. Reece, and J. T. Ruderman, J. High Energy Phys. 07 (2016) 016.
[39] C. Han, K. i. Hikasa, L. Wu, J. M. Yang, and Y. Zhang, J. High Energy Phys. 10 (2013) 216.
[40] A. Kobakhidze, N. Liu, L. Wu, J. M. Yang, and M. Zhang, Phys. Lett. B **755**, 76 (2016).
[41] M. Drees and J. S. Kim, Phys. Rev. D **93**, 095005 (2016).
[42] C. Han, J. Ren, L. Wu, J. M. Yang, and M. Zhang, Eur. Phys. J. C **77**, 93 (2017).
[43] G. H. Duan, K. i. Hikasa, L. Wu, J. M. Yang, and M. Zhang, arXiv:1611.05211.
[44] C. Han, K. i. Hikasa, L. Wu, J. M. Yang, and Y. Zhang, arXiv:1612.02296.
[45] ATLAS Collaboration, Report No. ATLAS-CONF-2013-049.
[46] V. Khachatryan *et al.* (CMS Collaboration), Eur. Phys. J. C **74**, 3036 (2014).
[47] G. Aad *et al.* (ATLAS Collaboration), J. High Energy Phys. 04 (2014) 169.
[48] V. Khachatryan *et al.* (CMS Collaboration), Phys. Rev. D **90**, 092007 (2014).
[49] J. Ellis and K. A. Olive, Eur. Phys. J. C **72**, 2005 (2012).
[50] H. Baer, V. Barger, and A. Mustafayev, J. High Energy Phys. 05 (2012) 091.
[51] G. Bélanger, G. Drieu La Rochelle, B. Dumont, R. M. Godbole, S. Kraml, and S. Kulkarni, Phys. Lett. B **726**, 773 (2013).
[52] M. Cahill-Rowley, R. Cotta, A. Drlica-Wagner, S. Funk, J. Hewett, A. Ismail, T. Rizzo, and M. Wood, Phys. Rev. D **91**, 055011 (2015).
[53] H. Fargnoli, C. Gnendiger, S. Paßehr, D. Stöckinger, and H. Stöckinger-Kim, J. High Energy Phys. 02 (2014) 070.
[54] S. Heinemeyer, W. Hollik, and G. Weiglein, Comput. Phys. Commun. **124**, 76 (2000).
[55] U. Chattopadhyay and A. Dey, J. High Energy Phys. 11 (2014) 161.
[56] K. A. Olive *et al.* (Particle Data Group Collaboration), Chin. Phys. C **38**, 090001 (2014).
[57] P. Bechtle, O. Brein, S. Heinemeyer, G. Weiglein, and K. E. Williams, Comput. Phys. Commun. **182**, 2605 (2011); **181**, 138 (2010).
[58] L. Calibbi, J. M. Lindert, T. Ota, and Y. Takanishi, J. High Energy Phys. 11 (2014) 106.
[59] M. Endo, K. Hamaguchi, T. Kitahara, and T. Yoshinaga, J. High Energy Phys. 11 (2013) 013.
[60] R. Arnowitt and P. Nath, Phys. Rev. D **46**, 3981 (1992).
[61] N. Arkani-Hamed, A. Delgado, and G. F. Giudice, Nucl. Phys. **B741**, 108 (2006).
[62] G. Belanger, F. Boudjema, P. Brun, A. Pukhov, S. Rosier-Lees, P. Salati, and A. Semenov, Comput. Phys. Commun. **182**, 842 (2011).
[63] H. Baer, A. Lessa, S. Rajagopalan, and W. Sreethawong, J. Cosmol. Astropart. Phys. 06 (2011) 031.
[64] P. A. R. Ade *et al.* (Planck Collaboration), Astron. Astrophys. **594**, A13 (2016).
[65] D. S. Akerib *et al.* (LUX Collaboration), Phys. Rev. Lett. **112**, 091303 (2014).
[66] D. S. Akerib *et al.*, Phys. Rev. Lett. **118**, 021303 (2017).
[67] A. Tan *et al.* (PandaX-II Collaboration), Phys. Rev. Lett. **117**, 121303 (2016).
[68] E. Aprile *et al.* (XENON1T Collaboration), Springer Proc. Phys. **148**, 93 (2013).
[69] C. Cheung, L. J. Hall, D. Pinner, and J. T. Ruderman, J. High Energy Phys. 05 (2013) 100.
[70] T. Han, F. Kling, S. Su, and Y. Wu, J. High Energy Phys. 02 (2017) 057.
[71] Report No. ATLAS-CONF-2016-075.
[72] Report No. CMS-PAS-SUS-16-024.
[73] Report No. CMS-PAS-SUS-16-022.
[74] G. Aad *et al.* (ATLAS Collaboration), Eur. Phys. J. C **76**, 259 (2016).
[75] W. Porod, Comput. Phys. Commun. **153**, 275 (2003).
[76] J. Alwall, R. Frederix, S. Frixione, V. Hirschi, F. Maltoni, O. Mattelaer, H.-S. Shao, T. Stelzer, P. Torrielli, and M. Zaro, J. High Energy Phys. 07 (2014) 079.
[77] T. Sjostrand, S. Mrenna, and P. Z. Skands, J. High Energy Phys. 05 (2006) 026.
[78] J. de Favereau, C. Delaere, P. Demin, A. Giammanco, V. Lemaître, A. Mertens, and M. Selvaggi, J. High Energy Phys. 02 (2014) 057.
[79] M. Cacciari, G. P. Salam, and G. Soyez, Eur. Phys. J. C **72**, 1896 (2012).
[80] M. Cacciari, G. P. Salam, and G. Soyez, J. High Energy Phys. 04 (2008) 063.
[81] M. Drees, H. K. Dreiner, J. S. Kim, D. Schmeier, and J. Tattersall, Comput. Phys. Commun. **187**, 227 (2015).
[82] W. Beenakker, R. Hopker, and M. Spira, arXiv:hep-ph/9611232.
[83] A. Barr and J. Scoville, J. High Energy Phys. 04 (2015) 147.
[84] P. Schwaller and J. Zurita, J. High Energy Phys. 03 (2014) 060.
[85] C. Han, A. Kobakhidze, N. Liu, A. Saavedra, L. Wu, and J. M. Yang, J. High Energy Phys. 02 (2014) 049.
[86] H. Baer, A. Mustafayev, and X. Tata, Phys. Rev. D **89**, 055007 (2014).
[87] C. Han, L. Wu, J. M. Yang, M. Zhang, and Y. Zhang, Phys. Rev. D **91**, 055030 (2015).
[88] B. Dutta, T. Ghosh, A. Gurrola, W. Johns, T. Kamon, P. Sheldon, K. Sinha, K. Wang, and S. Wu, Phys. Rev. D **91**, 055025 (2015).
[89] B. Dutta, W. Flanagan, A. Gurrola, W. Johns, T. Kamon, P. Sheldon, K. Sinha, K. Wang, and S. Wu, Phys. Rev. D **90**, 095022 (2014).
[90] N. Arkani-Hamed, T. Han, M. Mangano, and L. T. Wang, Phys. Rep. **652**, 1 (2016).
[91] M. Low and L. T. Wang, J. High Energy Phys. 08 (2014) 161.